Modeling of the Residence Time Distribution in a Buss Kneader with a Back-Propagation Neural Network

Chao Bi, Bo Jiang, Ao Li

College of Mechanical and Electrical Engineering, Beijing University of Chemical Technology, Beijing 100029, People's Republic of China

Received 7 May 2007; accepted 8 February 2008
DOI 10.1002/app.28251
Published online 2 May 2008 in Wiley InterScience (www.interscience.wiley.com).

ABSTRACT: With a back-propagation neural network, the residence time distribution (RTD) characteristics in a buss kneader were modeled on a series of experimental RTD data measured by a digital image processing method. The operating conditions (screw speed and feed rate) were chosen as the inputs of the network. The four-layered back-propagation neural network predicted not only the RTD character indices, including the shortest delay time, mean residence time, and variance of distribution, but also the complete RTD curve. On the basis of the mean residence time, the average degree of fill in the extruder was also calculated. Furthermore, the effects of the operating conditions on the RTD and average degree of fill were analyzed. The method provided herein can also be used to predict RTDs in other kinds of extrusion equipment. © 2008 Wiley Periodicals, Inc. J Appl Polym Sci 109: 2224–2231, 2008

Key words: modeling; extrusion

INTRODUCTION

In recent years, buss kneaders[1–12] have been increasingly used for compounding and mixing plastics and fibers. The degree of mixing or extent of degradation of a material intensively depends on how long it is exposed to the processing conditions. A material fed into the extruder simultaneously will leave the die at a different time. This leads to the problem of the residence time distribution (RTD) of the material inside the equipment. The concept of RTD, introduced first by Danckwerts[13] in 1995, is a useful tool for analyzing the flow situation inside an apparatus. The RTD function [$E(t)$] and the accumulated RTD function [$F(t)$] are often used to quantify the RTD character: $E(t)dt$ describes the fraction of flow at the exit that has spent time between time t and $t + dt$ in the system, and $F(t)$ shows the fraction of flow that has left the system at time t. According to the definitions of Levenspiel,[14] these two functions can be calculated with the following formulas:

$$E(t) = \frac{C(t)}{\sum_0^\infty C(t)\Delta t} \tag{1}$$

$$F(t) = \sum_0^t E(t)\Delta t \tag{2}$$

where $C(t)$ is the trace concentration measured at the exit of the extruder. In addition, two moments, the mean residence time (MRT) and variance of distribution (VOD), are defined as follows:

$$\mathrm{MRT} = \sum_0^\infty t \cdot E(t)\Delta t \tag{3}$$

$$\mathrm{VOD} = \sum_0^\infty (t - \mathrm{MRT})^2 \cdot E(t)\Delta t \tag{4}$$

The shortest delay time (SDT), which indicates the shortest time that a material spends inside the extruder, is also an important index for describing the RTD. It is defined as the time interval between the addition of the tracer and the first detection of the tracer at the exit of the extruder.

Furthermore, MRT can also be defined as the ratio of the actual filled volume of the equipment to the volume flow rate:

$$\mathrm{MRT} = \frac{\mathrm{ADF} \times V}{Q_v} \tag{5}$$

where V is the total volume of the reactor, ADF is the average degree of fill, and Q_v is the ratio of the mass flow rate (Q_m) to the density of the fluid (ρ). Thus, once V, MRT, Q_m, and ρ are available, ADF for a specified operating condition can be calculated.

The three main approaches to measuring the RTD are the offline method,[15–23] inline method,[24–30] and

Correspondence to: C. Bi (bichao812@sohu.com).
Contract grant sponsor: Young Teacher Natural Science Research Foundation of the Beijing University of Chemical Technology; contract grant number: QN0509.

online method.[31,32] It is well known that the traditional offline method is quite time-consuming and yields few data points, which are not enough to allow for a detailed analysis at the tail region of the RTD curves. In the cases of inline and online measurements, these problems are lessened, but the precise probes and data acquisition systems cost too much to be accepted commonly. The digital image processing (DIP) method is one of the offline RTD measurement methods, but it is much less labor-consuming than the traditional offline ones and cheaper than the inline or online ones. Enough data can be obtained by the DIP method to describe the long-tail phenomena of RTD curves. This method has been used in food processing.[23] The feasibility of the DIP method in measuring the RTD in a plasticating extruder has been studied in our previous work.[33]

To predict the RTD in the extrusion process, which is an intensely nonlinear system, it is necessary to build an appropriate mathematical model. In general, there are two ways to build the RTD models, including the hydromechanic method[34–39] and the chemical reaction engineering method.[14–19,24,25,40–42] In the hydromechanic method, the RTD in the extruder is derived on the basis of a precise velocity field analysis, for which an overall understanding of the screw geometry, dynamic and thermal conditions, and rheological properties of the materials is required. On the basis of the velocity field, after the calculation of the flow trajectories of the material points from the entrance to the exit inside the screw elements, the RTD in the screw elements can be analyzed by a statistical method. Because of the limit in the capability of the computer, the velocity field in a whole screw is not available commonly. Thus, a convolution technique[43] is employed to assemble the RTD for the entire apparatus on the basis of the statistically independent hypothesis.[44] In the chemical reaction engineering method, two kinds of ideal reactors (a plug flow reactor and a continuously stirred tank reactor) are connected to construct a conceptual flow model that represents the main features of the actual flow in the extruders according to the screw construction and processing mechanism. The flow patterns include the positive transport zone, mixing zone, dead volume, bypass, backflow, recirculating loops, and segregated flows and their combinations.[14] A number of models have been developed for single-screw extruders,[40] twin-screw extruders,[19,41] and buss kneaders.[42]

The precondition for modeling RTD by the two aforementioned approaches is an exact description of the flow and mixing mechanics of the equipment. Although many researchers have thrown themselves into studies of the flow and mixing mechanics of buss kneaders,[2–12] the studies on this topic are still at the beginning stage. Furthermore, in analyzing the velocity field and the mixing process, simplifications and hypotheses are absolutely necessary and unavoidably lead to differences between the actual situation and the simulated results.

In the work described herein, an experimental study was performed to measure the RTD in a buss kneader by the DIP method. The effects of the operating conditions on the RTD were analyzed. Based on MRT, ADF in the buss kneader was calculated. The effects of the operating conditions on ADF were also analyzed. The objective of this article is to present the application of a back-propagation neural network (BPNN) in modeling the RTD in a buss kneader. A great advantage of neural network models is that it is not necessary to know the mathematical relationship. Instead, they determine these relationships through successive training. With the help of BPNN, the complex relationship between the operating conditions and RTD in the buss kneader can be treated as a black box. The method provided herein can also be used to predict the RTD in other kinds of extrusion equipment.

EXPERIMENTAL

In this study, a DIP method was used to measure the RTD in a locally made JXW46 buss kneader (Jinwo Chemical Equipment Co., Nanjing, China) at different screw speeds (100, 150, 200, 250, and 300 rpm) and feed rates (5, 7.5, 10, 12.5, and 15 kg/h). As illustrated in Figure 1, the buss kneader was composed of three main parts: a reciprocating pin/barrel single-screw extruder with a rotating and oscillating modular screw, a melt gear pump system that was used to improve the steadiness of the extrusion, and a die mounted at the exit of the gear pump. The outer diameter of the screw was 45 mm, and the length/diameter ratio was 21. The functions of the EZ (conveying), KE (mixing), ST (restriction ring adaptor), and CF (continuous flight) elements in the screw were conveying, mixing, building pressure for melting with the help of the restriction ring element, and building pressure at the screw head to provide enough pressure for the gear pump, respectively.

The matrix polymer and the tracer used herein were low-density polyethylene with a 0.919–0.923 g/cm^3 density and a melt flow index of 1.8–3.2 g/10 min (2102TN00, Sinopec QiLu Co., Ltd., Zibo, China) and a red dye master batch that was precompounded with 20 parts of red dye and 100 parts of the matrix material (by weight percentage) and chopped into a size similar to that of the low-density polyethylene, respectively.

During the extrusion process, after a steady state was reached, a small amount of the dye master tracer was instantaneously fed into the buss kneader,

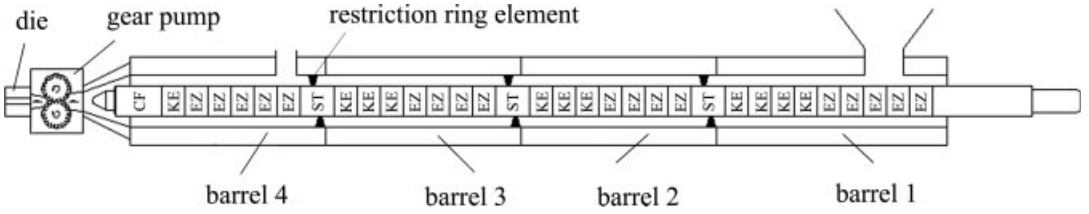

Figure 1 Schematic diagram of the screw configuration in the buss kneader.

and the extrudate was collected until there was no red color in the sample. After extrusion, the samples under each operating condition were placed on a black background. Then, a picture was taken with an Olympus C-60 digital camera (Olympus Co., Tokyo, Japan) with no flash in a room with a constant color temperature and illumination to ensure that all the pictures were taken in the same surrounding environment. The maximum number of available pixels of the digital camera was 6,000,000. The pictures were all taken in the 2816 pixel × 2112 pixel size and stored in the TIFF mode.

The color space of these pictures was RGB, which is a device-dependent color system, so it was converted into the device-independent $L^*a^*b^*$ color space in this process. After the background was separated, the variation of the average value of the red color intensity of all the pixels in the vertical direction for each piece with time was calculated. Then, the red color intensity/time curves were plotted on the basis of the data combining all of the red color intensities along the length of the extrudate for a specific operating condition. After the reduction of the noise and calibration of the baseline, the RTD was plotted. The experiments were repeated three times for a special operating condition, and the average results were used to train/validate the BPNN model. A detailed introduction about this method can be found in our previous work.[33]

NONLINEAR REGRESSION OF THE EXPERIMENTAL RTD CURVE

In time-dependent extrusion, such as reactive extrusion, MRT represents the average level of the reaction, VOD is a measure of the spread of the reaction extent around the average level, and SDT stands for the least degree of reaction. However, the complete RTD can show a detailed profile of the reaction extent, so the prediction of the complete RTD is more necessary than predictions of SDT, MRT, and VOD.

If a mathematical model is capable of fitting the experimental RTD data with a high correlation coefficient (R^2) between the predicted and experimental results, the model parameters estimated by nonlinear regression from the experimental data can be used to quantify the characteristics of the RTD curves.

The Zusatz function, which is a three-parameter RTD model and has a high ability to fit RTD data,[26] was employed in this study. This function can be expressed as follows:

$$C_z(t) = a \cdot \left(\frac{b}{t}\right)^{(c+1)} \exp\left[\left(\left(\frac{b}{t}\right)^{c} - 1\right) \cdot \left(\frac{-c-1}{c}\right)\right] \quad (6)$$

where a, b, and c are adjustable parameters that are related to the shape of the curve and $C_z(t)$ corresponds to $C(t)$ in eqs. (1) and (2). Thus, the $E_z(t)$ and $F_z(t)$ equations of the Zusatz function can be obtained according to the following definitions:

$$E_z(t) = \frac{C_z(t)}{\sum_0^\infty C_z(t)\Delta t} \quad (7)$$

$$F_z(t) = \sum_0^t E_z(t)\Delta t \quad (8)$$

The $F(t)$ function is monotone, increasing with a shape simpler to that of the $E(t)$ function, so it was applied for a fast rate of constringency in the nonlinear regression. Herein, the nonlinear regression was performed with the statistics toolbox of Matlab software (version 6.5.1) on the basis of the experimental data to estimate the model parameters, which are listed in Table I. As shown in this table, the differences among all of the a values was quite small, so an average value ($\bar{a}$) was used to replace a, and the same was done for parameter c. On the basis of the average values $\bar{a}$ and $\bar{c}$, the model parameter b was estimated again, and the result was denoted b', which is also listed in Table I. The R^2 values between the experimental and predicted $F(t)$ curves by $\bar{a}$, b', and $\bar{c}$ were all more than 0.95. Figures 2 and 3 show that the experimental and predicted $E(t)$ curves basically overlapped each other, and this indicates that the Zusatz function with parameters $\bar{a}$, b', and $\bar{c}$ has the ability to describe the RTD characteristics in a buss kneader. The application of Zusatz functions with parameters $\bar{a}$, b', and $\bar{c}$ means the reduction of outputs in the BPNN, and this is helpful in lessening the difficulty in building the BPNN

TABLE I
Regressed Parameters

Experiment	Feed rate (kg/h)	Screw speed (rpm)	Zusatz function parameters				
			a	*b*	*c*	*b′*	*b″*
1	5	100	0.979	289.531	8.853	289.419	289.201
2	5	150	0.974	272.308	9.110	271.608	271.884
3[a]	5	200	0.976	258.422	8.146	259.923	260.251
4	5	250	0.997	253.797	9.099	253.168	253.156
5	5	300	1.001	235.021	9.647	233.624	233.652
6	7.5	100	0.997	217.477	8.949	217.209	217.127
7[a]	7.5	150	1.002	196.840	8.623	197.158	198.372
8	7.5	200	1.008	187.379	8.523	187.845	188.249
9	7.5	250	1.007	182.312	8.509	182.792	182.917
10	7.5	300	1.008	174.222	8.309	175.024	174.991
11[a]	10	100	1.001	184.236	7.820	185.742	186.391
12	10	150	1.005	164.204	8.705	164.353	164.818
13	10	200	1.013	155.188	9.158	154.815	153.367
14	10	250	0.999	145.636	8.424	146.133	145.975
15	10	300	1.011	139.300	7.189	141.310	141.130
16	12.5	100	1.000	172.310	9.121	171.866	171.612
17	12.5	150	1.011	145.241	8.916	145.105	145.621
18	12.5	200	1.009	128.910	8.674	129.063	129.684
19	12.5	250	0.990	121.306	8.539	121.589	121.483
20[a]	12.5	300	1.023	119.467	8.468	119.824	118.758
21	15	100	1.013	162.557	8.722	162.657	162.756
22	15	150	0.991	131.498	9.229	131.050	130.777
23	15	200	1.011	110.321	8.228	110.853	110.862
24[a]	15	250	0.995	102.092	8.924	101.992	101.425
25	15	300	1.025	98.786	8.858	98.748	98.962
Average value			1.002		8.670		

[a] Used for validation of the ANN model.

model. However, one can find that the Zusatz function with parameters $\bar{a}$, b', and $\bar{c}$ cannot capture some irregularities of the experimental RTD curves, and this is a limitation of this function in fitting the experimental data of a buss kneader to some extent.

BPNN

Artificial neural networks (ANNs), which consist of a large number of simple processing elements called neurons and have a highly interconnected structure similar to that of brain cells of human neural networks, are considered artificial intelligence modeling techniques.[45,46] With ANN technology, we can solve some real-world problems for which it is very difficult to define a conventional algorithm. BPNN is the most popular type of ANN because it is easy to implement and fast and efficient to operate. Once the architecture of the network is determined,

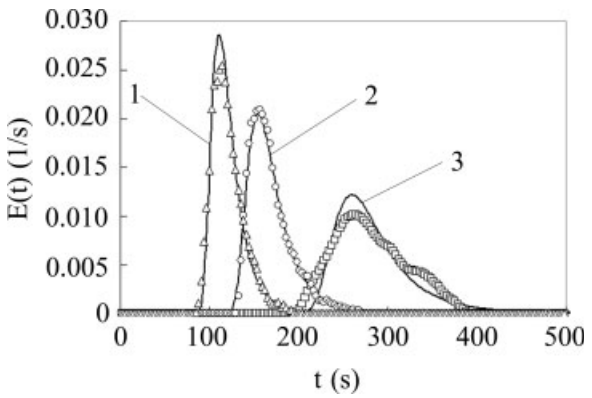

Figure 2 Effects of the feed rate on RTD at the same screw speed of 200 rpm: (1,△) 15, (2,○) 10, and (3,□) 5 kg/h. The discrete data are for the experimental results, and the continuous curves are for the predicted results.

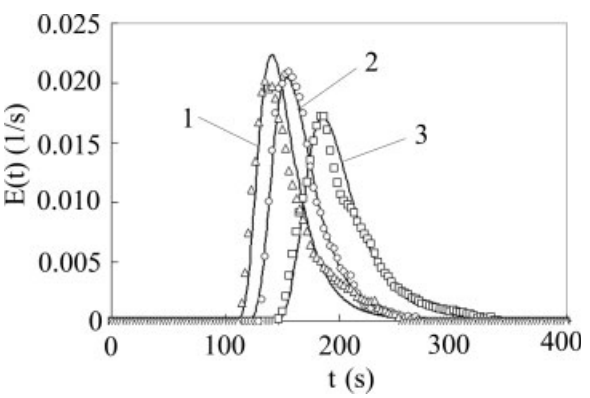

Figure 3 Effects of the screw speed on RTD at the same feed rate of 10 kg/h: (1,△) 300, (2,○) 200, and (3,□) 100 rpm. The discrete data are for the experimental results, and the continuous curves are for the predicted results.

through a series of supervised learning and validating processes, BPNN will have the ability to predict the result for unseen input.

Preprocessing of the data set

Inputs and outputs of BPNN must be numerical and between zero and one. For the best results, the output should be limited in the interval [0.05, 0.95]; otherwise, the network will not converge easily. Therefore, input and output samples for training and validating the network were preprocessed by the normalization technique according to the following formulas:

$$\bar{X}_i = \frac{X_i - X_{i\min}}{X_{i\max} - X_{i\min}} \tag{9}$$

$$\bar{Y}_i = \frac{Y_i - Y_{i\min}}{Y_{i\max} - Y_{i\min}} \times d_1 + d_2 \tag{10}$$

where $X_{i\max}$ and $X_{i\min}$ are the maximum and minimum of the ith input data X_i, respectively; $\overline{X}_i$ is the normalized value of X_i; $Y_{i\max}$ and $Y_{i\min}$ are the maximum and minimum of the ith output data Y_i, respectively; $\overline{Y}_i$ is the normalized value of Y_i; and the constants d_1 and d_2 are 0.90 and 0.05, respectively.

Output values that resulted from BPNN were converted to their equivalent values with the reverse method of normalization.

BPNN modeling

The job of choosing the appropriate network architecture for a specific problem is more art than science. Generally, the experimental data set is divided into a training set (A) and a validating set (B). For the sake of selecting the best network architecture, set A is subdivided into two subsets: one to train the network (A1) and another to validate the network (A2). Then, different network architectures are trained with set A1, and their performance is evaluated on A2. If the difference between the experimental and predicted values of A2 is less than the set value, the network architecture is acceptable. Besides the required precision, the rate of convergence is also an important index for determining the network architecture. After the network architecture is selected, the network is retrained on set A. At last, the generalization ability of the network is tested on set B. For the required precision in the validating set, the network can be trained again and again with different initial connection weights between the neurons.

As shown in Figure 4, a four-layered neural network was used for learning in this study. The network consisted of an input layer, two hidden layers, and an output layer. For input variables, we selected the screw speed and feed rate. The outputs that resulted from BPNN were SDT, MRT, VOD, and parameter b' of the Zusatz function. A typical sigmoidal neuron, which is one of the most widely used neurons, was employed in the hidden layer. The sigmoid transfer function is shown by

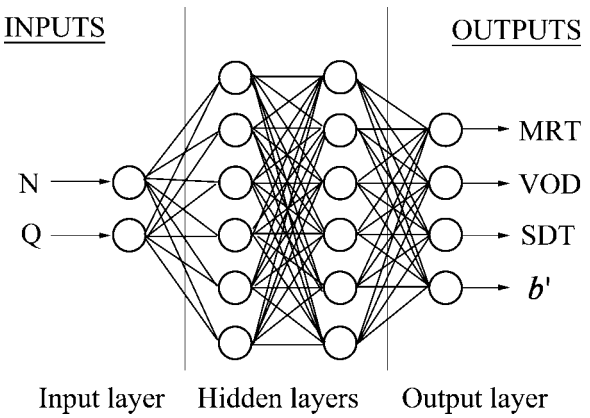

Figure 4 Structure of the four-layered neural network used in this study (N = screw speed; Q = feed rate).

$$f_s(x) = 1/[1 + \exp(-x)] \tag{11}$$

where f_s and x are a transfer function and a variable, respectively. Furthermore, the transfer function between the hidden layer and the output layer was a linear function (f_l), which can be expressed as follows:

$$f_l(x) = x \tag{12}$$

The BPNN connection weights were optimized with a supervised back-propagation algorithm based on the gradient–descent technique. The accuracy of the BPNN model was evaluated with a relative root mean square error (RRMSE) and the R^2 values, which were calculated with the following expressions:

$$\mathrm{RRMSE} = \sqrt{\sum_{i=1}^{m}\sum_{j=1}^{n}\left(Y_{ij}^{me} - Y_{ij}^{pr}\right)^2 \Big/ \sum_{i=1}^{m}\sum_{j=1}^{n}\left(Y_{ij}^{me}\right)^2} \tag{13}$$

$$R_i^2 = 1 - \frac{\sum_{j=1}^{n}\left(Y_{ij}^{me} - Y_{ij}^{pr}\right)^2}{\sum_{j=1}^{n}\left(Y_{ij}^{me}\right)^2} \text{ for the } i\text{th output} \tag{14}$$

where Y^{me}, Y^{pr}, m, and n are the measured value, predicted value, number of network outputs, and

TABLE II
Volumes of Parts

Part	Volume (cm^3)
KE element	24.086
EZ element	19.932
ST element	20.345
CF element	44.274
Gear pump	99.856
Die	5.655

number of data in the validating set for a single output, respectively. The ANN toolbox of Matlab software (version 6.5.1) was employed in the modeling of the BPNN.

RESULTS AND DISCUSSION

Effects of the operating conditions on the RTD

As stated by Hoppe et al.,[42] the RTD in a buss kneader has a bimodal character because of the original working principle and the back-flow of the polymer. Figures 2 and 3 show that in this study the fluctuating phenomena in the RTD curves are also obvious, especially at a low feed rate and a low screw speed. Furthermore, these two figures also illustrate the effects of the operating conditions on the RTD in the extruder: for a given screw speed, as the feed rate increases, a larger throughput results in a sharper RTD curve and a shorter SDT, and for a given feed rate, as the screw speed increases, we observe a shift of the RTD toward a shorter time. Additionally, we also can see that the effect of the feed rate on the RTD is larger than that of the screw speed.

Effects of the operating conditions on the ADF

On the basis of three-dimensional models, the volumes of the die, gear pump, and screw elements, of which the buss kneader is composed, were calculated with SolidWorks software (version 2004) and are listed in Table II. The ADFs were calculated with eq. (5) from the experimental MRTs, for which the density of the polymer was equal to 0.921 g/cm^3. Figure 5 shows the changes in ADFs with increasing screw speed at different feed rates. From this figure, we find that with an increase in the feed rate or decrease in the screw speed, ADF increases. When the screw speed is 100 rpm and the feed rate is 15 kg/h, ADF is close to 1. This indicates that the extruder with the screw configuration shown in Figure 1 is basically fully filled under this operating condition and that the conveying capability of the screw at a screw speed of 100 rpm is approximated to 15 kg/h; an increase in the feed rate will result in leakage flow from the venting port.

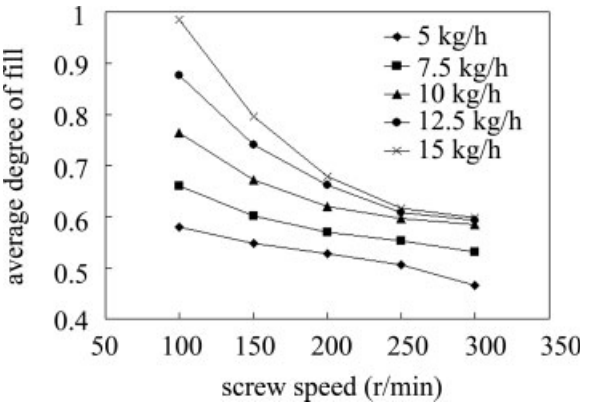

Figure 5 Changes in ADF with the screw speed at different feed rates.

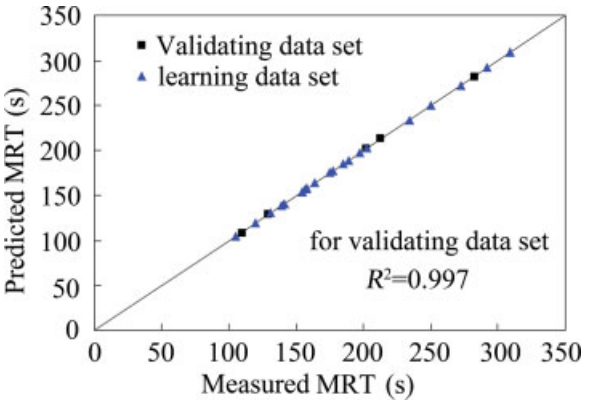

Figure 6 Correlation between measured and predicted MRTs. [Color figure can be viewed in the online issue, which is available at www.interscience.wiley.com.]

Predicting RTD by a BPNN

In the 25 experimental sets, 20 data sets (80%) were selected for learning, and the 5 remaining data sets

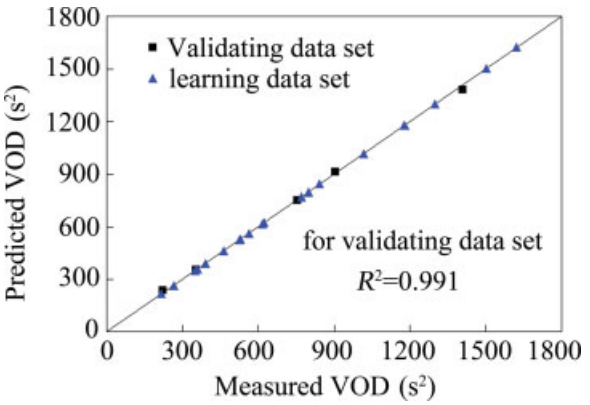

Figure 7 Correlation between measured and predicted VODs. [Color figure can be viewed in the online issue, which is available at www.interscience.wiley.com.]

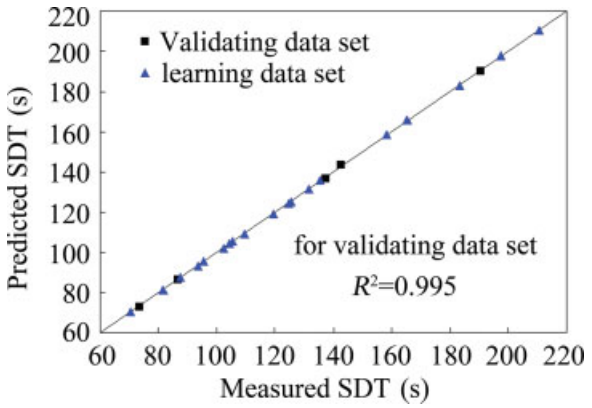

Figure 8 Correlation between measured and predicted SDTs. [Color figure can be viewed in the online issue, which is available at www.interscience.wiley.com.]

(20%) were used for validation of the ANN model. It is generally considered desirable to use at least 10% of all data sets for the validation of a model. The RRMSE of the final network for the validating data set was 0.015. Figures 6–8 show the correlation between measured and predicted MRTs, VODs, and SDTs, respectively. The R^2 values between the measured and predicted values were all larger than 0.99. The parameter b' was also forecast by the BPNN and labeled b'' (see Table I). Thus, on the basis of the Zusatz function with parameters $\bar{a}$, b'', and $\bar{c}$, one can draw the RTD curves for different operating conditions. Figures 9 and 10 show the differences between the predicted and experimental $E(t)$ and $F(t)$ curves, respectively. Although differences exist, the R^2 values between the experimental and predicted curves for both $E(t)$ and $F(t)$ curves are all higher than 0.95, which is an acceptable level for industrial applications. Table I shows that the differences between the model parameters b' and b'' are quite small, so it can be concluded that the differences between the experimental and predicted curves are mainly caused by the fitness of the Zusatz function. Thus, a more accurate prediction of the complete RTD needs a more appropriate function to fit the experimental data. Furthermore, the ADFs calculated from the predicted and experimental MRTs also have a high R^2 value (see Fig. 11). These aspects all confirm that the BPNN model has the ability to predict the RTD in a buss kneader.

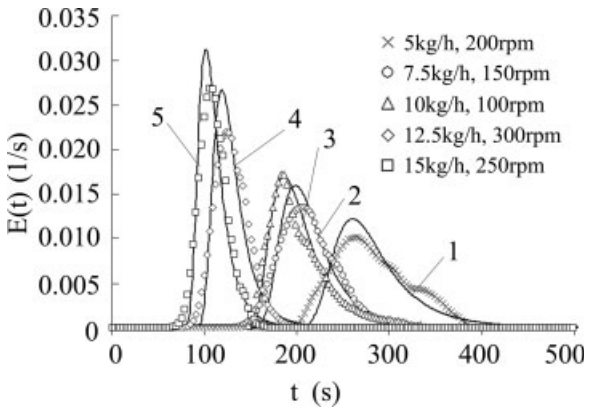

Figure 9 Comparison of predicted and experimental $E(t)$ curves: (1) feed rate = 5 kg/h and screw speed = 200 rpm, (2) feed rate = 7.5 kg/h and screw speed = 150 rpm, (3) feed rate = 10 kg/h and screw speed = 100 rpm, (4) feed rate = 12.5 kg/h and screw speed = 300 rpm, and (5) feed rate = 15 kg/h and screw speed = 250 rpm. The discrete data are for the experimental results, and the continuous curves are for the predicted results.

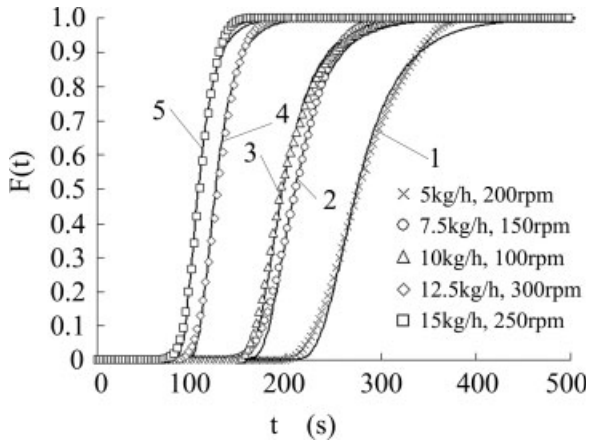

Figure 10 Comparison of predicted and experimental $F(t)$ curves: (1) feed rate = 5 kg/h and screw speed = 200 rpm, (2) feed rate = 7.5 kg/h and screw speed = 150 rpm, (3) feed rate = 10 kg/h and screw speed = 100 rpm, (4) feed rate = 12.5 kg/h and screw speed = 300 rpm, and (5) feed rate = 15 kg/h and screw speed = 250 rpm. The discrete data are for the experimental results, and the continuous curves are for the predicted results.

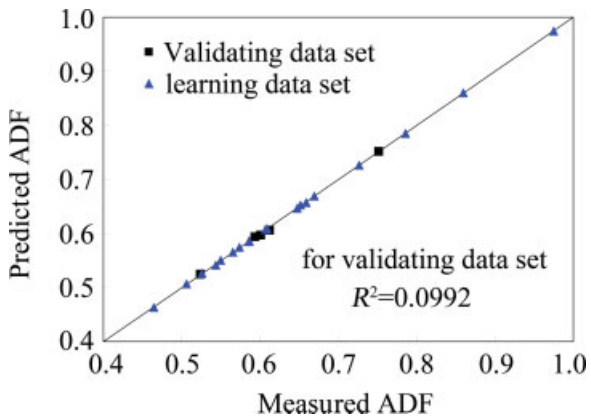

Figure 11 Correlation between measured and predicted ADFs. [Color figure can be viewed in the online issue, which is available at www.interscience.wiley.com.]

CONCLUSIONS

A supervised ANN trained by back-propagation algorithms was developed to predict the RTD and ADF in a buss kneader from operating conditions based on a series of RTD experimental data measured by the DIP method. From the results presented here, it is proved that the BPNN can be used with satisfactory accuracy for the prediction of the RTD characteristics in a buss kneader. Also, it has been demonstrated that the BPNN can be used instead of the simulation of mathematical models of RTD. This study will help application engineers to determine the performance of buss kneaders easily without requiring exhaustive experiments, thus saving both funds and time. Finally, the method described in this article can also be used to predict RTDs in other kinds of extrusion equipment.

The authors express their sincere thanks to friends (A. Li, Q. Dong, W. Lin, J. P. Wang, and N. B. Huang) for their help and discussions during the entire process of writing this article.

References

1. Wu, T. Q.; Jiang, B.; Wang, C. F. China Plast 2002, 16, 70.
2. White, J. L.; Lyu, M. Y. Polym-Plast Technol Eng 1998, 37, 385.
3. Wu, T. Q.; Jiang, B.; Xu, S. H. China Plast 2002, 16, 7.
4. Lyu, M. Y.; White, J. L. Polym Eng Sci 1998, 38, 1366.
5. Hoppe, S.; Detrez, C.; Pla, F. Polym Eng Sci 2002, 42, 771.
6. Elemans, P. H. M.; Meijer, H. E. H. Polym Eng Sci 1990, 30, 893.
7. Lyu, M. Y.; White, J. L. Int Polym Process 1995, 10, 305.
8. Lyu, M. Y.; White, J. L. Int Polym Process 1996, 11, 208.
9. Lyu, M. Y.; White, J. L. Int Polym Process 1997, 12, 104.
10. Lyu, M. Y.; White, J. L. J Reinforced Plast Compos 1997, 16, 1445.
11. Lyu, M. Y.; White, J. L. Polym Eng Sci 1997, 37, 623.
12. Lyu, M. Y.; White, J. L. J Reinforced Plast Compos 2000, 19, 756.
13. Danckwerts, P. V. Chem Eng Sci 1995, 50, 3857.
14. Levenspiel, O. Chemical Reaction Engineering; Wiley: New York, 1972.
15. Yeh, A. I.; Jaw, Y. M. J Food Eng 1999, 39, 81.
16. Chuang, G. C. C.; Yeh, A. I. J Food Eng 2004, 63, 21.
17. Seker, M. J Food Eng 2005, 67, 317.
18. Todd, D. B. Polym Eng Sci 1975, 15, 437.
19. Ruyck, H. D. J Food Eng 1997, 32, 375.
20. Kembłowski, Z.; Sęk, J. Polym Eng Sci 1981, 21, 1194.
21. Cassagnau, P.; Mijangos, C.; Michel, A. Polym Eng Sci 1991, 31, 772.
22. Ainsworth, P.; Ibanoglu, S.; Hayes, G. D. J Food Eng 1997, 32, 101.
23. Kumar, A.; Ganjyal, G. M.; Jones, D. D.; Hanna, M. A. J Food Eng 2006, 75, 237.
24. Puaux, J. P.; Bozga, G.; Ainser, A. Chem Eng Sci 2000, 55, 1641.
25. Wolf, D.; White, D. H. AIChE J 1976, 22, 122.
26. Zhang, X. M.; Xu, Z. B.; Feng, L. F.; Song, X. B. Polym Eng Sci 2006, 46, 510.
27. Gendron, R.; Daigneault, L. E.; Tatibouët; J.; Dumoulin, M. M. Adv Polym Technol 1996, 15, 111.
28. Mélo, T. J. A.; Canevarolo, S. V. Polym Eng Sci 2002, 42, 170.
29. Gilmor, C.; Balke, S. T.; Calidonio, F.; Rom-Roginski, A. Polym Eng Sci 2003, 43, 356.
30. Sun, Z.; Jen, C. K.; Shih, C. K.; Denelsbeck, D. A. Polym Eng Sci 2003, 43, 102.
31. Hu, G. H.; Kadri, I.; Picot, C. Polym Eng Sci 1999, 39, 930.
32. Carneiro, O. S.; Covas, J. A.; Ferreira, J. A.; Cerqueira, M. F. Polym Test 2004, 23, 925.
33. Bi, C.; Jiang, B. Polym Eng Sci 2007, 47, 1108.
34. Pinto, G.; Tadmor, Z. Polym Eng Sci 1970, 10, 279.
35. Lidor, G.; Tadmor, Z. Polym Eng Sci 1976, 16, 450.
36. Joo, J. W.; Kwon, T. H. Polym Eng Sci 1993, 15, 959.
37. Chen, L.; Lindt, J. T. AIChE J 1996, 42, 1525.
38. Bravo, V. L.; Hrymak, A. N.; Wright, J. D. Polym Eng Sci 2004, 44, 779.
39. van den Einde, R. M.; Kroon, P.; van der Goot, A. J.; Boom, R. M. Polym Eng Sci 2005, 45, 271.
40. Yeh, A. I.; Jaw, Y. M. J Food Eng 1998, 35, 211.
41. Gao, J.; Walsh, G. C.; Bigio, D.; Briber, R. M.; Wetzel, M. D. AIChE J 1999, 45, 2541.
42. Hoppe, S.; Detrez, C.; Pla, F. Polym Eng Sci 2002, 42, 771.
43. Cheng, P. Q. Digital Signal Processing; TsingHua University Press: Beijing, 2003.
44. Chen, L. Q.; Hu, G. H. AIChE J 1993, 39, 1558.
45. Yuan, C. R. Artificial Neural Network and Application; TsingHua University Press: Beijing, 1999.
46. Kumar, S. Neural Networks; TsingHua University Press: Beijing, 2006.